Check for updates

View Article Online
View Journal

Dalton Transactions

Accepted Manuscript

This article can be cited before page numbers have been issued, to do this please use: Y. Hou, H. An, B. Ding and Y. Li, *Dalton Trans.*, 2017, DOI: 10.1039/C7DT01302G.

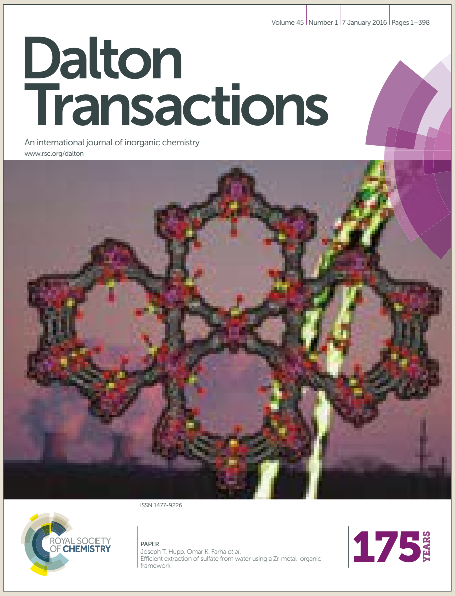

Volume 45 Number 1 7 January 2016 Pages 1–398

Dalton Transactions

An international journal of inorganic chemistry

www.rsc.org/dalton

ISSN 1477-9226

ROYAL SOCIETY OF CHEMISTRY

PAPER
Joseph T. Hupp, Omar K. Farha et al.
Efficient extraction of sulfate from water using a Zr-metal–organic framework

175 YEARS

This is an Accepted Manuscript, which has been through the Royal Society of Chemistry peer review process and has been accepted for publication.

Accepted Manuscripts are published online shortly after acceptance, before technical editing, formatting and proof reading. Using this free service, authors can make their results available to the community, in citable form, before we publish the edited article. We will replace this Accepted Manuscript with the edited and formatted Advance Article as soon as it is available.

You can find more information about Accepted Manuscripts in the author guidelines.

Please note that technical editing may introduce minor changes to the text and/or graphics, which may alter content. The journal's standard Terms & Conditions and the ethical guidelines, outlined in our author and reviewer resource centre, still apply. In no event shall the Royal Society of Chemistry be held responsible for any errors or omissions in this Accepted Manuscript or any consequences arising from the use of any information it contains.

ROYAL SOCIETY OF CHEMISTRY

rsc.li/dalton

View Article Online
DOI: 10.1039/C7DT01302G

Journal Name

ARTICLE

Evans-Showell-type polyoxometalate constructing novel 3D inorganic architectures with alkaline earth metal linkers: syntheses, structures and catalytic properties

Received 00th January 20xx,
Accepted 00th January 20xx

DOI: 10.1039/x0xx00000x

www.rsc.org/

Yujiao Hou, Haiyan An*, Baojun Ding, Yanqin Li

Four new architectures containing $[Co_2Mo_{10}H_4O_{38}]^{6-}$ polyoxoanions, $(C_2N_2H_{10})_2[Sr(H_2O)_5][Co_2Mo_{10}H_4O_{38}]\cdot 2H_2O$ **1**, $(C_2N_2H_{10})_2[Ba(H_2O)_3][Co_2Mo_{10}H_4O_{38}]\cdot 3H_2O$ **2**, $(C_3N_2H_{12})_2[Sr(H_2O)_5][Co_2Mo_{10}H_4O_{38}]\cdot 3H_2O$ **3** and $(C_3N_2H_{12})[Ba(H_2O)_4][Ba(H_2O)_4][Co_2Mo_{10}H_4O_{38}]\cdot 2H_2O$ **4** ($C_2N_2H_{10}$ = ethylenediamine; $C_3N_2H_{12}$ = 1,3-propanediamine) have been synthesized and characterized by elemental analysis, IR spectroscopy, solid diffuse reflective spectroscopy, TG analysis, powder X-ray diffraction and single crystal X-ray diffraction. Compounds **1** and **2** achieved in the presence of ethylenediamine, are built up of Evans-Showell-type anions $[Co_2Mo_{10}H_4O_{38}]^{6-}$, linked by Sr^{2+} or Ba^{2+} cations form 3D frameworks. To our knowledge, compound **1**(**2**) represents the first example of 3D architectures in which the Evans-Showell anions $[Co_2Mo_{10}H_4O_{38}]^{6-}$ were linked by pure alkaline earth cations. When propanediamine was used instead of ethylenediamine, compounds **3** and **4** with 2D network were obtained. phenomenon indicates that the organic cations which adjust the reaction pH values, can induce different dimensional inorganic frameworks. As heterogeneous catalysts, compounds **1**–**4** show excellent catalytic performance in the cyanosilylation of carbonyl compounds. Furthermore, these catalytic reactions were performed under solvent-free conditions using only a low amount of the catalysts, and these catalysts can be recovered and reused without displaying any significant loss of activity. As far as we know, compounds **1**–**4** represent the first examples of cyanosilylation catalyzed by POM-based species containing alkaline earth cations.

Introduction

Polyoxometalates (POMs), as inorganic high nuclear metal oxides (mainly Mo, W, V, Nb and Ta), have been an increasingly important topic, owing to their intriguing architectures and numerous potential applications in catalysis, medicine, electronics, magnetism and optics.[1-8] Over the past decade, many chemists from various disciplines have redirected their efforts to the field of three-dimensional (3D) extended frameworks based on POMs through suitable linkers, not only from a structural point of view but also from the significant applications of 3D materials which range from catalysis, chemical separation and gas storage.[9-18] However, 3D solid materials built up of POM building blocks are inclined to be linked by metal-organic coordination fragments.[19] So far, very few of 3D frameworks constructed from POMs are achieved through the all-inorganic elements, which are able to endow solid materials with new structures and composite properties. Therefore, choosing appropriate POMs and metal linkage units to achieve functional assemblies is a promising way to get new types of 3D inorganic framework materials possessing both stability and versatility.

Evans-Showell-type POM $[Co_2Mo_{10}H_4O_{38}]^{6-}$ with two terminal oxygen atoms, seized our attention, not merely holding strong coordination ability forming new inorganic architectures, but also possessing highly catalytic properties as Lewis acid-base catalysts.[20] To the best of our knowledge, only one example of 3D architectures based on $[Co_2Mo_{10}H_4O_{38}]^{6-}$ has been reported by our group: $[Ln(H_2O)_7][Ln(H_2O)_5][Co_2Mo_{10}H_4O_{38}]\cdot 5H_2O$ (Ln = Gd, Tb).[21] Meanwhile, the cheap alkaline earth metal cations not only hold the similar radius and coordination nodes with rare earth metal cations, but have potential applications as catalysts, scintillators, laser and fluorescent lamp.[22-26] Thus, constructing 3D inorganic framework compounds with excellent catalytic properties based on Evans-Showell-type POM $[Co_2Mo_{10}H_4O_{38}]^{6-}$ linked by alkaline earth metal cations, is still an appealing and challenging work.

Cyanosilylation of carbonyl compounds yields cyanohydrin ether, which is an important intermediate for fine chemicals and pharmaceuticals.[27,28] Hence, to design and synthesize efficient catalysts for cyanosilylation of carbonyl compounds is a meaningful

---

College of Chemistry, Dalian University of Technology, Dalian 116023, P. R. China
Email:anhy@dlut.edu.cn; Fax:+86-411-84657675; Tel:+86-411-84657675

Electronic Supplementary Information (ESI) Polyhedron view of the 1D homochiral chain of 1 and 3, 1D nonchiral chain of 2 and 4; polyhedral representation of the coordination modes of Sr cations in 1 and 3; coordination modes of Ba cations in 2 and 4; IR, TG curves, PXRD and CV curves patterns for 2–4, IR spectra for as-synthesized and recovered catalyst 1 and 3 are available. Study on recycling of catalyst 1 and 3 is listed in Table S3. Crystal data and structure refinement for 1–4 in Table S1. Selected bond lengths (Å) and angles (°) for 1–4 in Table S2. Cyanosilylation of aldehydes catalyzed by different POM-based compounds in Table S4

View Article Online
DOI: 10.1039/C7DT01302G

issue in current research. So far, the cyanosilylation is mostly catalyzed by electrophilic and nucleophilic catalysts, such as, phosphines, phosphazanes, and alkaline earth metal oxides.[29,30] Examples of cyanosilylation reaction catalyzing by POMs are very rare up to the present date. In 2012, Mizuno and coworkers firstly used polyoxoanion $[\{Y(H_2O)_2\}_2(\alpha\text{-}SiW_{10}O_{36})_2]^{10-}$ as a Lewis acid-base catalyst, which showed excellent catalytic effect for cyanosilylation of ketones and aldehydes with trimethylsilyl cyanide (TMSCN). In the same year, their group introduced a series of rare earth cations with larger ionic radii into the bilacunary $[\{Ln(H_2O)_2(acetone)\}_2(\alpha\text{-}SiW_{10}O_{36})_2]^{10-}$ (Ln = Y^{3+}, Nd^{3+}, Eu^{3+}, Tb^{3+}, or Dy^{3+}), to improve the catalytic performance of cyanosilylation of carbonyl compounds with TMSCN as homogeneous catalysts.[33] In 2014, Niu's group took advantage of $[H_2W_{11}O_{38}]^{8-}$ as building block to obtain a Lewis acid-base heterogeneous catalyst $\{[Cu_2(bpy)(H_2O)_{5.5}]_2[H_2W_{11}O_{38}]_3H_2O\cdot 0.5CH_3CN\}$, which can drive cyanosilylation with good performance.[35] In 2015, Sun and coworkers successfully isolated one inorganic-organic hybrid compound $\{[Cu_{12}(pbtz)_2(Hpbtz)_2(OH)_4(H_2O)_{16}][Na(H_2O)P_5W_{30}O_{110}]\}\cdot 16H_2O$, which can also catalyze cyanosilylation reactions through a heterogeneous manner.[36] Recently, our group reported compounds containing $[Co_2Mo_{10}H_4O_{38}]^{6-}$ as heterogeneous catalysts: $[Ln(H_2O)_5][Ln(H_2O)][Co_2Mo_{10}H_4O_{38}]\cdot 6H_2O$ (Ln = Sm, Eu) and $[Zn_2(H_2O)_5(4,4'\text{-bipy})_3]H_2[Co_2Mo_{10}H_4O_{38}]\cdot 5H_2O$ exhibit excellent catalytic effect under solvent-free conditions in the cyanosilylation reactions.[20] From the above researches, the development of efficient and cheap heterogeneous catalysts for cyanosilylation of carbonyl compounds with TMSCN still is a significant work in current researches. Meanwhile, POM-based catalysts for cyanosilylation reactions mainly utilized rare earth cations or transition metal cations as Lewis acid catalytic sites to date. In view of the similar radius of alkaline earth metals with rare earth metal cations, it is thus of considerable interest to investigate whether POM-based compounds containing alkaline earth metal cations can effectively catalyze the cyanosilylation reaction as heterogeneous catalysts.

Taking account of these, we took advantage of $[Co_2Mo_{10}H_4O_{38}]^{6-}$ as building blocks and alkaline earth metal cations as linkers, and expected to construct 3D inorganic frameworks with excellent catalytic effect of cyanosilylation reaction. Fortunately, we successfully obtained four compounds, namely $(C_2N_2H_{10})_2[Sr(H_2O)_5][Co_2Mo_{10}H_4O_{38}]\cdot 2H_2O$ **1**, $(C_2N_2H_{10})_2[Ba(H_2O)_3][Co_2Mo_{10}H_4O_{38}]\cdot 3H_2O$ **2**, $(C_3N_2H_{12})_2[Sr(H_2O)_5][Co_2Mo_{10}H_4O_{38}]\cdot 3H_2O$ **3** and $(C_3N_2H_{12})[Ba(H_2O)_4][Ba(H_2O)_4][Co_2Mo_{10}H_4O_{38}]\cdot 2H_2O$ **4**. Compounds **1** and **2** are obtained in the presence of ethylenediamine, which represent the first examples of 3D covalent structures based on Evans-Showell-type polyoxoanion and alkaline earth metal cations. Compounds **3** and **4** are got in the presence of propanediamine, exhibiting interesting 2D covalent networks. As the first Lewis acid-base catalysts based on POMs and alkaline metal cations, all four compounds show excellent performance in the cyanosilylation of carbonyl compounds and allow the reaction to be performed under solvent-free conditions using only a low amount of the catalysts, which can be recovered and reused without displaying any significant loss of activity.

Experimental section

Materials and methods

All chemicals were commercially purchased and used without further purification. $(NH_4)_6[Co_2Mo_{10}H_4O_{38}]\cdot 7H_2O$ was synthesized according to the literatures,[38,39] and characterized by means of IR spectroscopy. Elemental analyses (C, H and N) were performed on a Perkin-Elmer 2400 CHN elemental analyzer; Co, Mo, Ba and Sr were analyzed on a PLASMA-SPEC (I) ICP atomic emission spectrometer. IR spectra were recorded in the range 400–4000 cm^{-1} on an Alpha Centaur FT/IR Spectrophotometer using KBr pellets. TG analyses were performed on a Perkin-Elmer TGA7 instrument in flowing N_2 with a heating rate of 10 ºC·min^{-1}. PXRD patterns of the samples were recorded on a Rigaku Dmax 2000 X-ray diffractometer with graphite monochromatized Cu−Kα radiation (λ = 0.154 nm) and 2θ varying from 5 to 50°. UV-vis spectra were acquired on an Analytik Jena SPECORD S600 spectrophotometer equipped with a diode-array detector and an immersible fiber-optic probe. Electrochemical data were obtained at room temperature using a BAS CV-50 W electrochemical analyzer equipped with a glassy-carbon working electrode, a Pt-wire auxiliary electrode, and a Ag/AgCl (3M NaCl) BAS reference electrode.

Experimental Measurements

Synthesis of$(C_2N_2H_{10})_2[Sr(H_2O)_5][Co_2Mo_{10}H_4O_{38}]\cdot 2H_2O$ (1)

In a typical synthesis procedure for **1**, a mixture of $Sr(NO_3)_2$ (0.0423 g, 0.2 mmol) and $(NH_4)_6[Co_2Mo_{10}H_4O_{38}]\cdot 7H_2O$ (0.2 g, 0.1 mmol) was dissolved in 15 mL water. Then, one drop of ethylenediamine were introduced dropwise into the system, the pH value of the mixture was adjusted to 3.0 using 4 mol L^{-1} HCl under stirring, and the solution was refluxed at 80 °C for 12 h. The filtrate was kept for two days under ambient conditions, and then dark green triangular shaped crystals of **1** were isolated in about 62% yield (based on Mo). Elemental analyses: Calcd for **1** Mo, 47.33; Co, 5.91; Sr, 4.33; C, 2.37; N, 2.76; H, 1.89 (%). Found: Mo, 47.63; Co, 5.72; Sr, 4.02; C, 2.65; N, 2.90; H, 1.63 (%). FTIR data (cm^{-1}): 3500(s), 3192(m), 1680(s), 1500(vs), 1315(w), 1085(w), 939(vs), 906(vs), 825(m), 640(vs), 605(vs) and 522(s).

Synthesis of $(C_2N_2H_{10})_2[Ba(H_2O)_3][Co_2Mo_{10}H_4O_{38}]\cdot 3H_2O$ (2)

The preparation of **2** was similar to that of **1** except that $Ba(NO_3)_2$ (0.0423 g, 0.2 mmol) was used instead of $Sr(NO_3)_2$ (0.0523g, 0.2 mmol). The pH value of the mixture was about 3.0. Dark green triangular shaped crystals of compound **2** were obtained in about 60% yield (based on Mo). Elemental analyses: Calcd for **2** Mo, 46.56; Co, 5.72; Ba, 6.66; C, 2.33; N, 2.72; H, 1.86 (%). Found: Mo, 46.91; Co, 5.55; Ba, 6.87; C, 2.01; N, 2.99; H, 1.56 (%). FTIR data (cm^{-1}): 3510(s), 3183(m), 1674(s), 1509(vs), 1313(w), 1082(w), 936(vs), 904(vs), 827(m), 642(vs), 607(vs) and 524(s).

Synthesis of $(C_3N_2H_{12})_2[Sr(H_2O)_5][Co_2Mo_{10}H_4O_{38}]\cdot 3H_2O$ (3)

The preparation of **3** was similar to that of **1** except that one drop of propanediamine were introduced dropwise into the system instead of ethylenediamine. The pH value of the mixture was about 2.8. Dark green rhomboid shaped crystals of compound **3** were obtained in about 61% yield (based on Mo). Elemental analyses: Calcd for **3** Mo, 46.19; Co, 5.67; Sr, 4.22; C, 3.47; N, 2.70; H, 2.33 (%). Found:

View Article Online
DOI: 10.1039/C7DT01302G

Mo, 46.01; Co, 5.79; Sr, 4.56; C, 3.22; N,2.89; H, 2.50 (%). FTIR data (cm^{-1}): 3490(s), 3153(m), 1654(vs), 1529(s), 1509(s), 1353(w), 926(vs), 894(vs), 827(w), 632(vs), 602(vs) and 514(w).

Synthesis of $(C_3N_2H_{12})[Ba(H_2O)_4][Ba(H_2O)_4][Co_2Mo_{10}H_4O_{38}]\cdot 2H_2O$ (4)

The preparation of **4** was similar to that of 3 except that $Ba(NO_3)_2$ (0.0423 g, 0.2 mmol) was used instead of $Sr(NO_3)_2$ (0.0523g, 0.2 mmol). The pH value of the mixture was about 2.7. Dark green prismatic shaped crystals of compound **4** were obtained in about 59% yield (based on Mo). Elemental analyses: Calcd for **4** Mo, 46.19; Co, 5.67; Ba, 4.22; C, 3.47; N, 2.70; H, 2.33 (%). Found: Mo, 46.01; Co, 5.79; Ba, 4.56; C, 3.22; N,2.89; H, 2.50 (%). FTIR data (cm^{-1}): 3453(m), 3063(m),1584(vs), 1500(w), 1383(vs), 926(vs), 894(w), 637(vs), 606(w) and 514(w).

X-Ray crystallography

The crystallographic data of all compounds were collected on the Bruker Smart CCD diffractometer with Mo Kα radiation(λ=0.71073 Å) by ω and θ scan modes. Empirical absorption correction was applied. The structures of **1–4** were solved by the direct method and refined by the Full-matrix least squares on F^2 using the SHELXTL-97 software.[37] All of the non-hydrogen atoms were refined anisotropically in **1–4**. The hydrogen atoms attached to water molecules were not located in **1–4**. The restraints such as 'isor' or 'dfix' were used in the refinements for obtaining reasonable atom sites and thermal parameters. A summary of the crystallographic data and structural determination for **1–4** is provided in Table S1.

CCDC reference numbers: 1542000-1542003 for compounds **1–4,** 1542889 for compound **5**.

Cyanosilylation

The detailed reaction conditions are shown in the captions of Table 1. A typical procedure for the cyanosilylation reaction of aldehyde is as follows: 2 mol% catalyst (**1–4**) was added to a mixture of aldehyde (0.5 mmol) and $(CH_3)_3SiCN$ (1.5 mmol), in the absence of solvent. The reaction mixture was stirred at room temperature under a N_2 atmosphere. The progress of the reaction was monitored by GC analysis. After the reaction was completed, the catalyst was removed by filtration and centrifugation of the reaction mixture. All products (cyanohydrin trimethylsilyl ethers) were confirmed by a comparison of their GC retention times, GC-MS spectra. GC analysis was performed using HP6890/5973MS with a cross-linked (95%)-dimethyl-(5%)-diphenylpolysiloxane column of 30 m length.

Results and discussion

Synthesis

The reaction of $(NH_4)_6[Co_2Mo_{10}H_4O_{38}]\cdot 7H_2O$ and Sr^{2+} or Ba^{2+} cations in the presence of ethylenediamine or propanediamine has been investigated. Four compounds with four kinds of structures were obtained. Compounds **1**(**2**) and **3**(**4**) were synthesized under the similar reaction conditions, except for the alternation of the organic cations. It is clear that the organic cations of the reaction system are the key factor influencing the structures and topologies of these compounds. In the presence of ethylenediamine, compounds **1** and **2** were separated, exhibiting a 3D microporous frame constructed from isolated $[Co_2Mo_{10}H_4O_{38}]^{6-}$ polyoxoanions, alkaline earth metal cations and protonated ethylenediamine. In the presence of propanediamine, two 2D structures **3** and **4** were isolated, which are constructed from isolated $[Co_2Mo_{10}H_4O_{38}]^{6-}$ polyoxoanions, alkaline earth metal cations and protonated propanediamine. To further study the influence of the organic cations, we also attempted to use other organic cations such as butanediamine and 1,2-propanediamine instead of ethylenediamine or 1,3-propanediamine under the similar reaction conditions, but we only got the raw materials $(NH_4)_6[Co_2Mo_{10}H_4O_{38}]\cdot 7H_2O$. Meanwhile, no crystals were obtained without the addition of organic cations under the similar conditions .

When other alkaline earth metal cations such as Mg^{2+} and Ca^{2+} were introduced to the reaction system, we only got compound **5**, which is constructed from isolated $[Co_2Mo_{10}H_4O_{38}]^{6-}$ and protonated organic cations (Fig. S5). This result may be because the ionic radii of Mg^{2+} and Ca^{2+} are smaller and their coordination ability is weaker than Sr^{2+} and Ba^{2+} with large ionic radii. The similar phenomenon that the differences of ionic radii of metal cations lead to different structures have been reported in the reaction system of POMs and rare earth metal cations.[20,21,40] Further, if organic cation was not added to the solution of Mg^{2+}/Ca^{2+} and POMs, only precipitation can be obtained. Alkaline metal cations (such as Na^+, K^+, Rb^+ and Cs^+) were also attempted to be introduced into the reaction system under the similar reaction conditions, but only raw materials $(NH_4)_6[Co_2Mo_{10}H_4O_{38}]\cdot 7H_2O$ were got. To probe the effect of the reaction condition, many parallel experiments were proceeded, which indicate that stoichiometry, pH value and reaction temperature can affect the quality of crystals. The products are apparently influenced by the stoichiometry of $Sr^{2+}(Ba^{2+})/[Co_2Mo_{10}H_4O_{38}]^{6-}$. Compounds **1**(**2**) and **3**(**4**) can be well isolated by the 2:1 $Sr^{2+}(Ba^{2+})/[Co_2Mo_{10}H_4O_{38}]^{6-}$ ratio. When the ratio was adjusted from 2:1 to 3:1 or 1:1, the crystal quality of the compounds was poor, and the yields were reduced. The optimal pH value is from 2.5 to 4.0. For a low pH (pH = 2), compound **5** was obtained; for a high pH (pH = 4.3) the raw materials $(NH_4)_6[Co_2Mo_{10}H_4O_{38}]\cdot 7H_2O$ were isolated. In addition, the best reaction temperature is 80 °C. At lower temperature (25 °C), no reaction occurred; at higher temperature (100 °C), crystals with poor quality can be obtained.

Crystal structures of 1 and 2

Single crystal X-ray diffraction analyses exhibit that compounds **1** and **2** crystallize in *C*c space group and display a unique 3D framework assembled by Evans-Showell-type polyoxoanions $[Co_2Mo_{10}H_4O_{38}]^{6-}$ and Sr^{2+} or Ba^{2+} cations. The structure of $[Co_2Mo_{10}H_4O_{38}]^{6-}$ can be deduced from the planar Anderson ion $[CoMo_6H_6O_{24}]^{3-}$ by removing one $\{MoO_5\}$ group from each of two $[CoMo_6H_6O_{24}]^{3-}$ ions, turning one ~45° around the anionic equatorial plane and joining them so that the two CoO_6 octahedra share an edge. In the polyoxoanion, four of the 10 crystallographically unique oxygen atoms surrounding the two Co^{3+} ions, are bound to hydrogen atoms, which are identified by the calculation of bond valence sums. Six kinds of oxygen atoms exist in the cluster according to the manner of oxygen coordination, that is

View Article Online
DOI: 10.1039/C7DT01302G

terminal oxygen Ot, terminal oxygen Ot′ linked to Sr^{2+}or Ba^{2+}, double-bridging oxygen Ob, central oxygen Oc (μ3-OH atom of a Co and two Mo atoms), central oxygen Od (μ4-O atom of a Co and three Mo atoms), central oxygen Oq (μ4-O atom of two Co and two Mo atoms). Thus the Mo–O bond lengths fall into six classes: Mo–Ot 1.692(4)–1.723(4) Å, Mo–Ot′ 1.713(5)–1.723(6) Å, Mo–Ob 1.878(4)–1.975(4) Å, Mo–Oc 2.226(4)–2.316(4) Å, Mo–Od 1.893(4)–2.347(3) Å and Mo–Oq 2.272(4)–2.308(4) Å in **1**; Mo–Ot 1.683(6)–1.724(6) Å, Mo–Ot′ 1.709(5)–1.712(4) Å, Mo–Ob 1.881(6)–1.979(5) Å, Mo–Oc 2.250(5)–2.311(5) Å, Mo–Od 1.987(5)–2.329(5) Å and Mo–Oq 2.272(5)–2.328(5) Å in **2**. The central Co–O distances are 1.869(3)–1.949(4) Å in **1** and 1.863(3)–1.960(5) Å in **2**, and the O–Co–O angles are in the range of 83.78(15)–175.80(16)° in **1** and 83.6(2)–176.2(2)° in **2**. All bond lengths and bond angles are within the normal ranges.[32,33]

Just as Fig. 1a, the asymmetric unit of compound **1** is composed of one crystallization-independent $[Co_2Mo_{10}H_4O_{38}]^{6-}$ anion, one Sr^{2+} cation and two protonated ethylenediamine. The Sr^{2+} cation is eight-coordinated, forming a double-capped trigonal prism coordination geometry, which was defined by five water molecules [Sr−OH_2 2.592(4)−2.643(4) Å] and three terminal oxygen atoms from three $[Co_2Mo_{10}H_4O_{38}]^{6-}$ units [Sr−O 2.574(4)−2.615(4) Å] (Fig. S1a). The average bond length of Sr−O bond is 2.599 Å. Similarly, the asymmetric unit of compound **2** is composed of one crystallization-independent $[Co_2Mo_{10}H_4O_{38}]^{6-}$ anion, one Ba^{2+} cation and two protonated ethylenediamine. The Ba^{2+} cation is seven-coordinated, forming a single-capped trigonal prism coordination geometry, which was defined by three water molecules [Ba−OH_2 2.804(8)−2.861(8) Å] and four terminal oxygen atoms from three $[Co_2Mo_{10}H_4O_{38}]^{6-}$ units [Ba−O 2.732(5)−2.984(6) Å] (Fig. S2a). The average bond length of Ba−O bond is 2.829 Å. It is noteworthy that compounds **1** and **2** both display 3D frameworks assembled by $[Co_2Mo_{10}H_4O_{38}]^{6-}$ polyoxoanions and Sr^{2+}/Ba^{2+} cations. To our best knowledge, compounds **1** and **2** represent the first examples of 3D architectures based on $[Co_2Mo_{10}H_4O_{38}]^{6-}$ units and alkaline earth metals, and the second examples of 3D architectures based on $[Co_2Mo_{10}H_4O_{38}]^{6-}$. In compound **1**, the chiral $[Co_2Mo_{10}H_4O_{38}]^{6-}$ clusters are linked by some Sr^{2+} ions to form 1D chiral chain (Fig. S1b), then adjacent opposite-handed chiral chains are interconnected by Sr^{2+} cations to produce a 2D nonchiral layer along the *a* axis (Fig. 2b). Furthermore, these 2D sheets are joined together *via* the Sr−O−Sr bonds to form a 3D framework (Fig. 2c). The resulting 3D framework contains 1D channels along the *b* axis. Each 1D channel splits into three smaller channels. Their dimensions are respectively ca. 3.0 × 6.7, 3.7 × 5.2, and 4.4 × 5.0 Å in **1** along the *b* axis. Free water molecules and ethylenediamine molecules are filled in the channels and coordinated water molecules are included into them. The solvent accessible volume of **1** and **2** after removal of the water molecules and ethylenediamine molecules are respectively about 20.5% and 20.9%, as determined by using PLATON. From the view of topology, the $[Co_2Mo_{10}H_4O_{38}]^{6-}$ unit is covalently bonded to three adjacent Sr cations, and each Sr cation is linked with three $[Co_2Mo_{10}H_4O_{38}]^{6-}$ units. Therefore, the overall 3D framework can be rationalized as a 3-connected net by assigning the $[Co_2Mo_{10}H_4O_{38}]^{6-}$ units and Sr ions as three connected node which are topologically equivalent nodes (Fig. 3). Careful examination indicated that the Schläfli symbol for this binodal network is 10^3, which is assigned to the (10,3)-d topology according to the literatures (Fig. 3). Interestingly, along the *c* axis, the topology of compound **1** consists of two different 1D helical chiral chains: right hand and left hand (Fig. 3d). Such intriguing architectures and topologies is very rare.

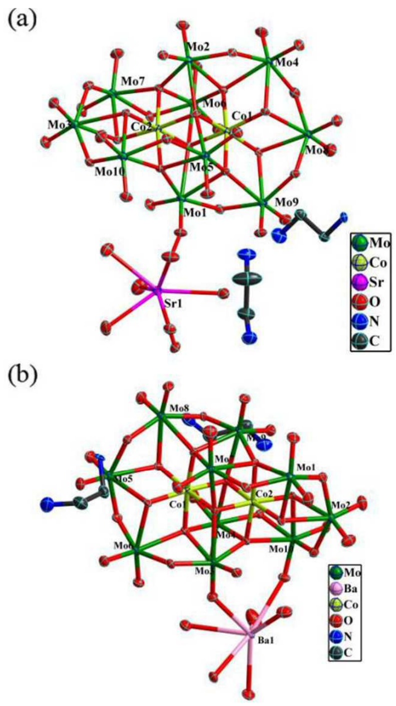

Fig. 1 (a) ORTEP drawing of **1** with thermal ellipsoids at 50% probability. (b) ORTEP drawing of **2** with thermal ellipsoids at 50% probability.(color code: Co, yellow; Mo, green; Sr, purple; Ba, pink; O, red).

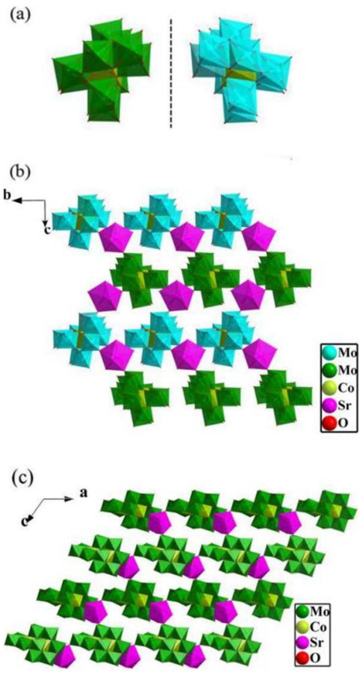

View Article Online
DOI: 10.1039/C7DT01302G

Fig. 2 (a) Polyhedral representation of two enantiomers of $[Co_2Mo_{10}H_4O_{38}]^{6-}$ polyoxoanion in **1**. (b) 2D nonchiral layer in **1**, showing the alternately arranged left-handed and right-handed chiral chains along the a axis (c) View along the a axis illustrating the 3D framework. Free water molecules are omitted for clarity. (color code: Co, yellow; Mo, green/blue; Sr, purple; O, red).

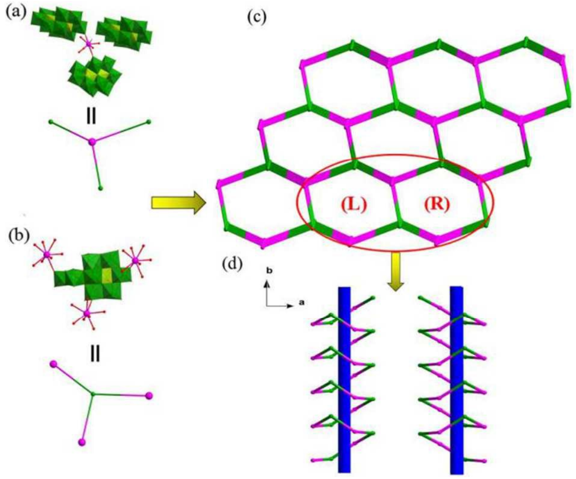

Fig. 3 (a) 3-Connected $[Co_2Mo_{10}H_4O_{38}]^{6-}$ unit coordinated with three Sr^{2+} cations. (b) 3-Connected Sr^{2+} node linked with three $[Co_2Mo_{10}H_4O_{38}]^{6-}$ clusters. (c) A schematic view of the 3D 3,3-connected network with the topology along the b axis. (d) Scheme of the 1D left-handed and right-handed chiral chain along the *c* axis.

Similarly, in compound **2**, the chiral $[Co_2Mo_{10}H_4O_{38}]^{6-}$ clusters are linked by some Ba^{2+} ions to form nonchiral 1D double chains (Fig. S2b). Next, the adjacent chains are joined together to form a 2D layer along the *b* axis (Fig. 4a). Then the 2D sheets are interconnected via the Ba−O−Ba bonds to form a 3D framework (Fig. 4b). From the view of topology, the $[Co_2Mo_{10}H_4O_{38}]^{6-}$ unit is covalently bonded to three adjacent Ba cations, and each Ba cation is linked with three $[Co_2Mo_{10}H_4O_{38}]^{6-}$ units. Therefore, the overall 3D framework can be also rationalized as a 3,3-connected net by assigning the $[Co_2Mo_{10}H_4O_{38}]^{6-}$ units and Ba cations as three connected node with Schläfli symbol of 10^3, as shown in Fig. 5. It is noteworthy that the topology of compound **2** is also made up of two different helical chiral chains: right hand and left hand (Fig. 5d).

So far, except for compounds **1** and **2**, only one example of 3D architectures based on $[Co_2Mo_{10}H_4O_{38}]^{6-}$ has been reported by our group: $[Ln(H_2O)_7][Ln(H_2O)_5][Co_2Mo_{10}H_4O_{38}]\cdot5H_2O$ (Ln = Gd, Tb).[21] Owing to the similar ionic radii between Sr^{2+} (Ba^{2+}) cations and rare earth metal cations, all these compounds have 3D frameworks. Compared 3D structures of compounds **1** and **2** with those of reported compounds, we found that different metal cations can produce different 3D structures. Compounds **1** and **2** crystallize in *C*c space group, while $[Ln(H_2O)_7][Ln(H_2O)_5][Co_2Mo_{10}H_4O_{38}]\cdot5H_2O$ crystallize in *P*2(1)/c space group. In $[Ln(H_2O)_7][Ln(H_2O)_5][Co_2Mo_{10}H_4O_{38}]\cdot5H_2O$, two unique Ln cations display two different coordination sphere. Ln(1) cation is nine-coordinated, forming a tricapped trigonal prism coordination environment, and Ln(2) cation, joined neighboring $[Co_2Mo_{10}H_4O_{38}]^{6-}$ polyoxoanions together as linker, displays a square antiprismatic geometry. However, the asymmetric unit of compounds **1**(**2**) both hold one metal cation Sr^{2+}(Ba^{2+}), and Sr^{2+} and Ba^{2+} cations show double-capped trigonal prism and single-capped trigonal prism coordination geometry, respectively. Owing to the different charges and different coordination modes of alkaline earth metal cations and rare earth metal caitons, compounds **1**(**2**) and reported species exhibit different 3D topological structures. From the view of topology, compounds $[Ln(H_2O)_7][Ln(H_2O)_5][Co_2Mo_{10}H_4O_{38}]\cdot5H_2O$ can be rationalized as a binodal 4-connected $SrAl_2$(sra) net by assigning the $[Co_2Mo_{10}H_4O_{38}]^{6-}$ units and Ln(1) ions as four connected node with Schläfli symbol of $4^2\cdot6^3\cdot8$. And topological analysis reveals that the simplified framework of compounds **1**(**2**) feature a 3,3-connected 3D network with the Schläfli symbol (10,3)-d, which consists of two different 1D helical chiral chains: right hand and left hand that is rare for POMs. Thus it can be seen that metal cations can affect structures of the compounds.

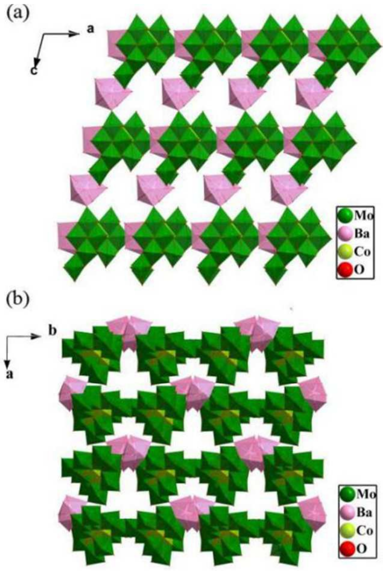

Fig. 4 (a) Polyhedron view of the 2D sheet along *b* axis in **2**. (b) View along the *c* axis illustrating the 3D framework in **2**. Free water molecules are omitted for clarity.(color code: Co, yellow; Mo, green/blue; Ba, pink; O, red).

View Article Online
DOI: 10.1039/C7DT01302G

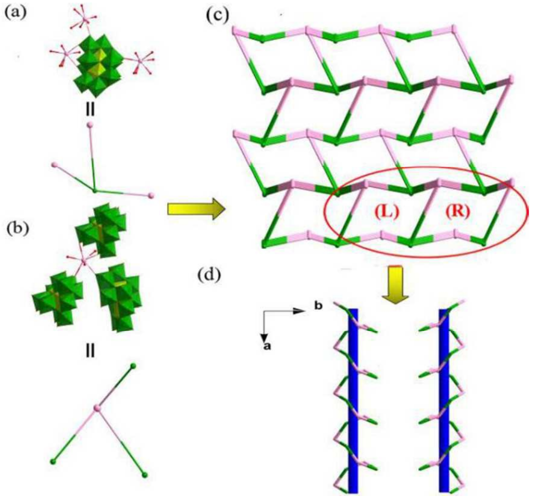

Fig. 5 (a) 3-Connected $[Co_2Mo_{10}H_4O_{38}]^{6-}$ unit coordinated with three Ba^{2+} cations. (b) 3-Connected Ba^{2+} node linked with three $[Co_2Mo_{10}H_4O_{38}]^{6-}$ clusters. (c) A schematic view of the 3D 3,3-connected network with the topology along the b axis. (d) Scheme of the 1D left-handed and right-handed chiral chain along the *c* axis.

Crystal structures of 3 and 4

When propanediamine was used instead of ethylenediamine under the similar conditions with compounds **1** and **2**, two different compounds **3** and **4** were isolated from the solution. Single crystal structural analysis reveals that compound **3** crystallizes in the space group *P*21/n. The asymmetric unit in the structure of **3** is composed of $[Co_2Mo_{10}H_4O_{38}]^{6-}$ polyoxoanion and one Sr^{2+} cation with two protonated propanediamine balancing the charges. Compound **4** crystallizes in the space group *P*-1, which is composed of $[Co_2Mo_{10}H_4O_{38}]^{6-}$ polyoxoanion and two Ba^{2+} cations with one protonated propanediamine balancing the charges, and it also plays a 2D network structure. The structure of $[Co_2Mo_{10}H_4O_{38}]^{6-}$ anion is as well an Evans-Showell type. According to the environment of the oxygen coordination, the oxygen atoms can divide into six kinds. Therefore, the bond lengths of Mo-O fall into six categories: Mo–Ot 1.688(5)–1.720(4) Å, Mo–Ot′ 1.696(5)–1.713(5) Å, Mo–Ob 1.872(4)–1.985(4) Å, Mo–Oc 2.254(4)–2.295(4) Å, Mo–Od 1.969(4)–2.412(4) Å and Mo–Oq 2.270(4)–2.344(4) Å in **3**. Mo–Ot 1.699(10)–1.754(9) Å, Mo–Ot′ 1.702(6)–1.725(9) Å, Mo–Ob 1.898(8)–1.975(9) Å, Mo–Oc 2.233(9)–2.281(8) Å, Mo–Od 1.991(8)–2.326(8) Å and Mo–Oq 2.297(8)–2.311(7) Å in **4**. The central Co–O distances are 1.859(4)–1.955(4) Å, and the O–Co–O angles are in the range of 84.11(18)–176.11(15)° in compound **3**. The central Co–O distances are 1.875(8)–1.958(8) Å, and the O–Co–O angles are in the range of 84.3(4)–174.3(3)° in compound **4**. And the bond lengths and bond angles are in agreement with the normal ranges, similar to compounds **1** and **2.**

The asymmetric unit in **3** is composed of one crystallographically independent Evans-Showell-type polyoxoanion linked by one Sr^{2+} anion with two protonated propanediamine. The Sr^{2+} cation exists in the nine coordination environment, forming a single-capped square antiprism coordination geometry (Fig. 6a), which are coordinated by five water molecules [$Sr{-}OH_2$ 2.524(5)−2.853(5) Å] and four terminal oxygen atoms from three $[Co_2Mo_{10}H_4O_{38}]^{6-}$ [Sr−O 2.641(4)−2.811(4) Å]. The average bonds length of Sr−O bond is 2.425 Å (Fig. S3a). Similarly, the asymmetric unit of **4** consists of one crystallographically independent polyoxoanion, two Ba^{2+} and one protonated propanediamine. The two Ba^{2+} cations exhibit different coordination environment. Ba1 exists in the six coordination environment, forming a distorted octahedron coordination geometry, and coordinates to four water molecules [$Ba{-}OH_2$ 2.707(5)−2.729(5) Å] and two terminal oxygen atoms from two $[Co_2Mo_{10}H_4O_{38}]^{6-}$ units [Ba−O 2.841(5)−2.850(5)Å]. Ba2 exists in the eight coordination environment, forming a double-capped trigonal prism coordination geometry, and coordinates to four water molecules [$Ba{-}OH_2$ 2.793(5)−2.876(5)Å] and four terminal oxygen atoms from four $[Co_2Mo_{10}H_4O_{38}]^{6-}$ units [Ba−O 2.738(5)−2.974(5) Å]. The average bond length of Ba-O bond is 2.845(5)Å (Fig. S4a, b).

Interestingly, both compounds of **3** and **4** show 2D network structures. In compound **3**, the chiral $[Co_2Mo_{10}H_4O_{38}]^{6-}$ clusters are linked by some Sr^{2+} ions to form a 1D chiral chain (Fig. S3b), then adjacent opposite-handed chiral chains are interconnected by Sr^{2+} cations to produce a 2D nonchiral layer along the *b* axis (Fig. 7a). It's worth noting that 2D sheets are interconnected by hydrogen bonds among polyoxoanions and nitrogen atoms of propanediamine (O···N 2.729-2.825Å in **3**) to develop a 3D supramolecular framework (Fig. 7b). Similarly, in compound **4**, the chiral $[Co_2Mo_{10}H_4O_{38}]^{6-}$ clusters are linked by some Ba^{2+} ions to form nonchiral 1D double chains (Fig. S4c). Next, the adjacent chains are joined together to form a 2D layer along *c* axis. Then 2D sheets are joined together by hydrogen bonds among polyoxoanions and nitrogen atoms of propanediamine (O···N 2.759-2.924Å in **4**) to develop a 3D supramolecular framework (Fig. 8).

Bond valence sum calculations show that all Mo atoms are in the +6 oxidation state, Co atoms are in the +3 oxidation state, and the alkaline earth metal cations are in the +2 oxidation state. These results are consistent with the charge balance considerations.[42]

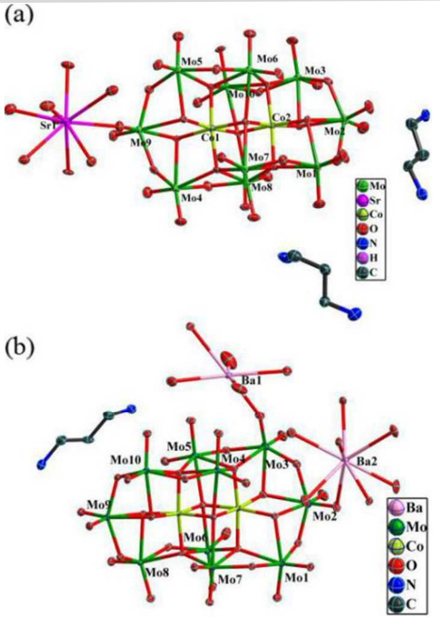

View Article Online
DOI: 10.1039/C7DT01302G

Fig. 6 (a) ORTEP drawing of **3** with thermal ellipsoids at 50% probability. (b) ORTEP drawing of **4** with thermal ellipsoids at 50% probability.(color code: Co, yellow; Mo, green; Sr, purple; Ba, pink; O, red).

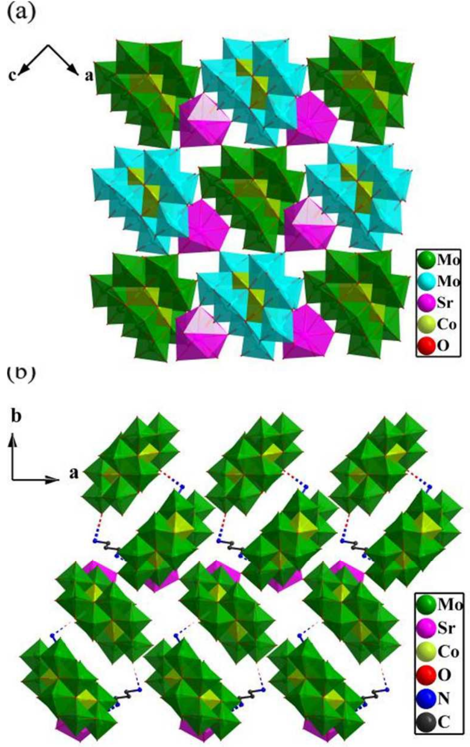

Fig. 7 (a) 2D nonchiral layer in **3**, showing the alternately arranged left-handed and right-handed chiral chains along the *b* axis. (b) View of the 3D supramolecular framework of **3** along the *c* axis. Free water molecules are omitted for clarity. (color code: Co, yellow; Mo, green/blue; Sr, purple; O, red)

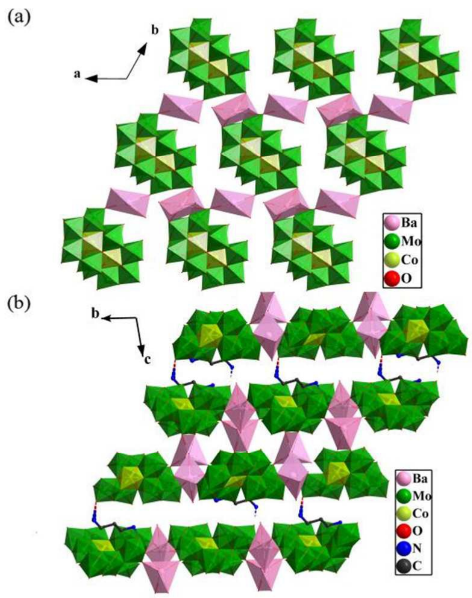

Fig. 8 (a) Polyhedron view of the 2D sheet along *b* axis. (b) View of the 3D supramolecular framework of **4** along the *c* axis. Free water molecules are omitted for clarity. (color code: Co, yellow; Mo, green; Ba, pink; O, red).

FT-IR spectroscopy and PXRD

In correspondence with the reported literatures, the IR spectra of compounds **1**-**4** show similar characteristic vibrational bands of the Evans-Showell-type structure $[Co_2Mo_{10}H_4O_{38}]^{6-}$ (Fig. S6). The terminal Mo–O units and the bridging Mo–O–Mo groups (M=Mo, Co) are located at 850–950 cm^{-1} and 580–690cm^{-1}, respectively. In addition, the bands at 3600−2800 cm^{-1} can be attributed to the stretching vibrations of O−H and N−H and 1700−1400 cm^{-1} can be correspond to the bending vibrations of the O−H and N−H. Below 500 cm^{-1}, the spectrum is rather difficult to analyze, the bending of the Mo−Ot and Mo−Ob bonds can be mixed with the Mo−Oc stretching vibrations. These results are in agreement with their single crystal structural analyses.

The PXRD patterns for **1**–**4** are presented in Fig. S7. The diffraction peaks of both calculated and experimental patterns match well, indicating the phase purities of these compounds. These conclusions are in agreement with the results of the single crystal X-ray analysis.

Thermal gravimetric (TG) Analysis

The TG curve of **1** is shown in Fig. S8a, which was carried out in the N_2 atmosphere within the scope of 30 to 800°C. According to the TG curve, we can know that **1** exhibits three weight loss steps, and the total weight loss is 16.0%, which meets the calculated weight loss of 15.7%. The first weight loss from 30 to 200°C is 5.0%, corresponding to all the lattice water and partial ethylenediamine. The second weight loss of 8.0% from 200 to 560°C, mainly attributes to the partial ethylenediamine and coordinated water (calc. 12.5%). The last weight loss of 2.7% from 570 to 800°C arises from the loss of oxygen molecules.

The TG curve of **2** is shown in Fig. S8b, which was carried out in the N_2 atmosphere within the scope of 30 to 700°C. According to the TG curve, we can know that **2** exhibits three weight loss steps, and the total weight loss is 16.4%, which meets the calculated weight loss of 16.0%. The first weight loss from 30 to 200°C is 4.7%, corresponding to all the lattice water and partial ethylenediamine. The second weight loss of 8.4% from 200 to 500°C, mainly attributes to the partial ethylenediamine and coordinated water (calc. 12.8%). The last weight loss of 3.6% from 500 to 700°C arises from the loss of oxygen molecules.

The TG curve of **3** is shown in Fig. S8c, which was carried out in the N_2 atmosphere within the scope of 30 to 800°C. According to the TG curve, we can know that **3** exhibits three weight loss steps, and the total weight loss is 17.3%, which meets the calculated weight loss of 17.6%. The first weight loss from 30 to 120°C is 3.0%, corresponding to all the lattice water and partial propanediamine. The second weight loss of 9.7% from 120 to 600°C, mainly attributes to the partial propanediamine and coordinated water(calc. 13.0%). The last weight loss of 4.6% from 600 to 800°C arises from the loss of oxygen molecules.

View Article Online
DOI: 10.1039/C7DT01302G

The TG curve of **4** is shown in Fig. S8d, which was carried out in the N_2 atmosphere within the scope of 30 to 800°C. According to the TG curve, we can know that **4** exhibits three weight loss steps, and the total weight loss is 13.4%, which meets the calculated weight loss of 13.1%. The first weight loss from 30 to 200°C is 3.9%, corresponding to all the lattice water (calc. 4.1%). The second weight loss of 5.6% from 200 to 500°C, mainly attributes to the partial propanediamine and coordinated water. The last weight loss of 4.6% from 500 to 800°C arises from the loss of remainder coordinated water and oxygen molecules.

UV-Vis spectroscopy

In order to get the absorption bands located in both the ultraviolet and visible regions, the diffuse reflectivity for solid samples of four compounds are shown in Fig. 9. The absorption (*A*) date were calculated from the reflectivity using the function: $A = \log(1/R\%)$ where R is the reflectivity at a given wavelength (λ). On the UV region (200-400 nm), there are two absorption bands at 224 nm, 305 nm for **1**, 223 nm, 304 nm for **2**, 225 nm, 303 nm for **3**, and 225 nm 303 nm for **4**, which are assigned to O→Mo charge transfer for $[Co_2Mo_{10}H_4O_{38}]^{6-}$ polyoxoanions. On the vision region (400-800 nm), the plots display two absorption bands at 441 nm, 607 nm for **1**, 440 nm, 605 nm for **2**, 442 nm, 607 nm for **3** and 441 nm, 604 nm for **4**, which were respectively assigned to the $^1A_{1g} \rightarrow {}^1T_{2g}$ and $^1A_{1g} \rightarrow {}^1T_{1g}$ transition of a regular octahedral configuration low-spin Co^{3+} in the $[Co_2Mo_{10}H_4O_{38}]^{6-}$ anion.[41]

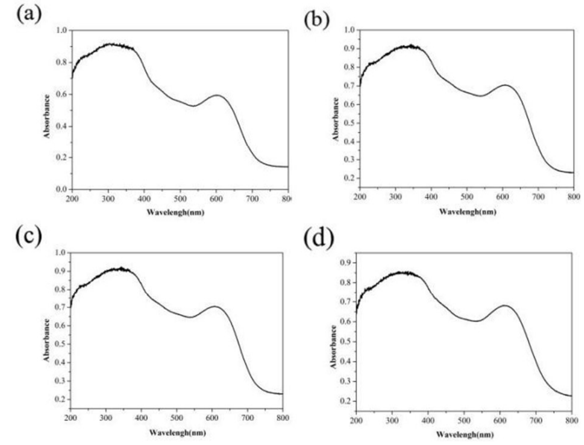

Fig. 9 (a) UV−vis diffuse reflectance spectra of bulk **1**. (b) UV−vis diffuse reflectance spectra of bulk **2**. (c) UV−vis diffuse reflectance spectra of bulk **3**. (d) UV−vis diffuse reflectance spectra of bulk **4.**

Electrochemistry studies

The electrochemical properties of **1**–**4** were investigated by cyclic voltammetry (CV) in a pH=4 (0.2 M CH_3COONa+CH_3COOH) buffer solution at different scan rates. Compound **1** was taken as a representative (as shown in Fig. 10). The cyclic voltammetric response was initially scanned in the positive direction from a starting potential of −1.2 V. For **1**, it can be clearly seen that in the potential range of +0.800 to -1.200 V, five redox peaks appear and the mean peak potentials are -0.80, -0.48, -0.32,-0.27 and +0.6 V (vs. the Ag/AgCl electrode), respectively. The first peak at -0.8V corresponds to the reduction of the molybdenum unit in the polyoxoanion framework, and the second peak at -0.48V is ascribed to the oxidation of molybdenum unit, which indicates that the reduction is irreversible. This is because Evans-Showell-type polyoxoanion contains two terminal cis-oxygen atoms which make the reduction process is irreversible. Similar phenomenon has been observed in other polyoxomolybdates with two terminal cis-oxygen atoms.[43,44] The third peak at -0.32V corresponds to the reduction of cobalt unit, and the last two anodic peaks at -0.27V and +0.6V belong to the oxidation of cobalt unit. The above domain where the waves are located is alike to other Co-based complexes.[45,46] The cyclic voltammograms reveal the presence of irreversible redox processes of molybdenum and cobalt units. This phenomenon is due to subsequent decomposition of the cluster, which was confirmed by the UV-Vis spectrum of the buffer solution (Fig S9). Furthermore, the CV curve from +0.6 to -0.6 V was detected (Fig S10), and the redox potentials Ⅲ Ⅵ Ⅴ can be seen, which thus can be ascribed to redox peaks of cobalt unit. If the measurement is cycled from +1.5 to -1.3 V, no other new peak appeared (Fig S11). For **1**, the cathodic peak potentials shift towards the negative direction and the anodic peak potentials to the positive direction with increasing scan rates from 25 to 400 mV s^{-1}. The peak currents are almost proportional to the scan rate, which indicate that the redox process are surface-controlled.[47-49] Compounds **2**–**4** exhibit similar CV curves with compound **1** at the scan rate from 25 to 400 mVs^{-1} (Fig S12).

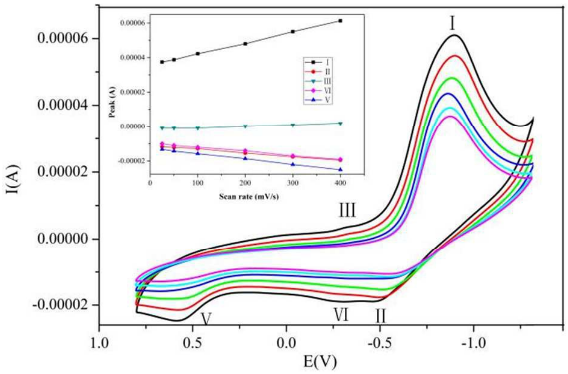

Fig. 10 The cyclic voltammograms of the **1** in pH 4 (0.2 M CH_3COONa +CH_3COOH) aqueous solution at different scan rates (from inner to outer: 25, 50, 100, 200, 300 and 400, mV s^{-1}). The inset shows the peak current versus the scan rate plot.

Catalysis study

Because of the importance of cyanohydrins as key intermediates in the synthesis of organic compounds, such as α-hydroxy acids, α-hydroxy aldehydes and β-aminoalcohols, the development of efficient catalysts for cyanosilylation is a very important subject in current research. Among the catalysts employed for the cyanosilylation reaction, both acid catalysts and base catalysts can act as catalysts to promote cyanosilylation. In addition, various cyanating reagents have been adopted in the synthesis of cyanohydrins, but trimethylsilyl cyanide (TMSCN) is the most widely used and safest cyanating regents for nucleophilic addition to

View Article Online
DOI: 10.1039/C7DT01302G

carbonyl compounds to give cyanohydrin trimethylsilyl ether.[33] In particular, it is expected that POMs with large negative charges can nucleophilically activate TMSCN, thus resulting in promotion of cyanosilylations, as observed for Lewis base catalyzed cyanosilylations. In this sense the starting substrates commonly used are aldehydes or ketones with TMSCN as the nucleophilic regent. Therefore, we detected the activity of compounds **1**–**4** as heterogeneous catalysnosilylation in the aldehyde cyanosilylation reaction under solvent-free condition at room temperature.

Firstly, we selected the cyanosilylation of benzaldehyde as a model reaction to evaluate the catalytic activities for compounds **1**–**4**. The reaction was carried out with 2 mol% of catalysts under the conditions describe in Table 1. All compounds effectively catalyzed the cyanosilylation to afford the corresponding cyanohydrin trimethysilyl ether with yield of up to about 99%. The catalytic effects of four compounds were compared with those of POMs reported in the literatures, displayed in detail in Table S4. In a comparison of the activity of our catalysts with that of some previous reported POM-based compounds, such as $[Ln(H_2O)_5][Ln(H_2O)_7][Co_2Mo_{10}H_4O_{38}]$ $6H_2O$ (Ln = Sm; Eu), $\{[Cu_2(bpy)(H_2O)_{5.5}]_2[H_2W_{11}O_{38}] \cdot 3H_2O \cdot 0.5CH_3CN\}$ and $\{[Cu_{12}(pbtz)_2(Hpbtz)_2(OH)_4(H_2O)_{16}][Na(H_2O)P_5W_{30}O_{110}]\}\cdot 16H_2O$, it was found to be less than the former two (benzaldehyde, 5h, yield = 98.4%), because the yield was 87% in the same time under similar reaction condition with compound **1** as catalyst. Although the yield of compound **1** was very close to the third compound, the third one need more time and uses solvent conditions (benzaldehyde, 24 h, yield = 98.1%). The last one need more time while the yield was far less than that of compound **1** (benzaldehyde, 24 h, and yield = 61.7%). Besides, in an equivalent ratio of compound **1** and **3**, compound **1** showed higher catalytic results than **3**. Given the fact that the similar composition between both compounds, the different catalytic activity may be ascribed to the different structures. As heterogeneous catalyst, compound **1** showing a 3D microporous framework may result in more exposure of the active sites than the 2D network structures in **3**.

Subsequently, various organic substrates containing aldehydes with different electronic effects are converted into the corresponding cyanosilylation products through the catalyzed reaction. With a substrate like 2-hydroxybenzaldehyde, 4-methylbenzaldehyde, or 4-nitrobenzaldehyde, the yield is high, too (Table 1). It indicates that the nature of the substituent on the aromatic ring didn’t dramatically affect the reaction yield. In contrast, a drastic decrease of catalytic activity occurred when substrate with the large steric hindrance was introduced, such as: 1-napthaldehyde. It reveals that the large steric hindrance of substrate makes the substrate hardly approach to the alkaline earth metal cations of the catalyst at the process of cyanosilylation reaction, leading to poor yield.

To further study the catalyst recyclability and stability in the catalytic process. The used catalysts were readily recovered from the catalytic reaction describe above by filtration. The filtrate of the reaction media showed no catalytic effect for the catalytic reaction of aldehyde. The isolated catalysts were reused at least three times without an appreciate loss of its high catalytic performance (from 99%–93.7%) (Table. S3). The PXRD patterns of retrieved catalysts were identical to those of the fresh catalysts(Fig. 11). The IR spectra of the recovered compounds **1** and **3** were also identical to those of the fresh prepared samples (Fig. S13). These observation indicated that **1** and **3** are true heterogeneous catalysts. Additionally, infrared spectroscopy of the compounds **1** and **3** impregnated with benzaldehyde showed one broad C-O stretch at 1688.7 and 1689.4 cm^{-1}, respectively. The *v*(C-O) stretch occurred a red shift of ~ 13.1 and 12.4 cm^{-1} from 1701.8 cm^{-1} of the free benzaldehyde (Fig. S14). The red shift illustrated the possible activation of the substrate by catalysts **1** and **3**. Furthermore, the control experiment for cyanosilylation of benzaldehyde with $[Co_2Mo_{10}H_4O_{38}]^{6-}$ precursor in a homogeneous manner gave 65.4% yield, which is far lower than that of **1** and **3** in the heterogeneous manner. The higher yields of **1** and **3** is possibly attributed to the synergistic effect of the Lewis acid (Sr^{2+} cations) and the Lewis base (surface oxygen atoms of the $[Co_2Mo_{10}H_4O_{38}]^{6-}$ POM) that activated respectively aldehydes and TMSCN at the same time.

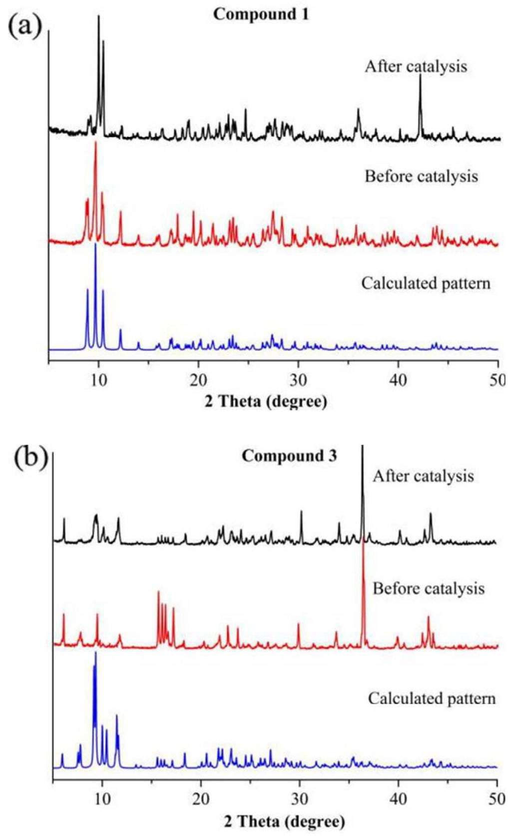

Fig. 11 (a) Powder X-ray diffraction (PXRD) patterns of **1** (b) Powder X-ray diffraction (PXRD) patterns of **3**: calculated pattern from crystal data (blue line); experimental pattern before catalysis (red line); recovered catalyst **1** or **3** after 3 catalytic runs of the cyanosilylation of benzaldehyde (black line).

View Article Online
DOI: 10.1039/C7DT01302G

Table 1 Cyanosilylation of aldehydes catalyzed by compounds **1**–**4**[a].

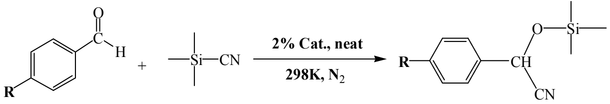

Compound	Aldehyde	Time (h)	Yield (%)[b]
1	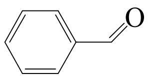	6	99.0
2		6	95.6
3		7	95.3
4		7	93.2
1	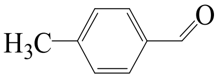	6	97
3		7	96.3
1	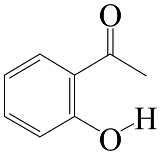	6	96.4
3		7	94.2
1	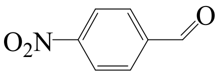	6	96.1
3		7	95.8
1	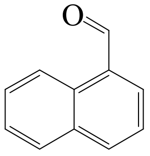	7	75.4
3		9	64.2
1	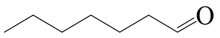	5	99.2
3		6	98.7
Blank	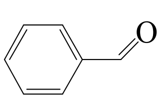	7	16.3
$(NH_4)_6[Co_2Mo_{10}H_4O_{38}]\cdot 7H_2O$		7	65.4

[a]Reaction conditions: catalyst 2 mol%, aldehyde 0.5 mmol, TMSCN 1.5 mmol, without solvent, room temperature (25 °C) under N$_2$. [b]Yields were determined by GC analysis using naphthalene as an internal standard.

Conclusions

In summary, we have successfully obtained two 3D frameworks and two 2D networks in the system of Evans-Showell-type polyoxoanions $[Co_2Mo_{10}H_4O_{38}]^{6-}$ and alkaline earth metal cations. Compounds **1** and **2** represent the first examples of 3D covalent structures based on Evans-Showell-type polyoxoanion and alkaline earth metal cations. Additionally, these compounds are efficient heterogeneous Lewis acid-base catalysts for cyanosilylation of carbonyl compounds under solvent-free conditions. To the best of our knowledge, this is the first time that inorganic 3D structures based on POMs and alkaline earth metal cations are used as catalysts in the cyanosilylation. Thus, the successful isolation of these compounds inspire us to develop new catalytic materials containing POMs and alkaline earth metal cations.

Acknowledgment

The authors thank the National Natural Science Foundation of China (21371027, 21274015, 21102013, 20901013), Natural Science Foundation of Liaoning Province (2015020232) and Fundamental Research Funds for the Central Universities (DUT15LK02, DUT15LN18, DUT16ZD205) for financial supports.

References

1 A. Müller, F. Peters, M. T. Pope and D. Gatteschi, *Chem. Rev.*, 1998, **98**, 239.
2 S. Uchida, M. Hashimoto and N. Mizuno, *Angew. Chem. Int. Ed.*, 2002, **42**, 2814.
3 D. L. Long, E. Burkholder and L. Cronin, *Chem. Soc. Rev.*, 2007, **36**, 105.
4 M. Li, C. Xu, J. S. Ren, E. B. Wang and X. G. Qu, *Chem. Commun.*, 2013, **49**, 11394.
5 J. Song, Z. Luo, D. K. Britt, H. Furukawa, O. M. Yaghi, K. L. Hardcastle and C. L. Hill, *J. Am. Chem. Soc.*, 2011, **133**, 16839.
6 Z. Y. Zhang, Q. P. Lin, D. Kurunthu, T. Wu, F. Zuo, S. T. Zheng, C. J. Bardeen, X. H. Bu and P. Y. Feng, *J. Am. Chem. Soc.*, 2011, **133**, 6934.
7 L. Chen, F. L. Jiang, Z. Z. Lin, Y. F. Zhou, C. Y. Yue and M. C. Hong, *J. Am. Chem. Soc.*, 2005, **127**, 8588.
8 A. Seliverstov, and C. Streb, *Chem. Commun.*, 2014, **50**, 1827.
9 J. S. Qin, D. Y. Du, W. Guan, X. J. Bo, Y. F. Li, L. P. Guo, Z. M. Su, Y. Y. Wang, Y. Q. Lan and H. C. Zhou, *J. Am. Chem. Soc.*, 2015, **137**, 7169.
10 H. J. Pang, J. Peng, C. J. Zhang, Y. G. Li, P. P. Zhang, H. Y. Ma, Z. M. Su, *Chem. Commun.*, 2010, **46**, 5097−5099.
11 J. Q. Shen, Y. Zhang, Z. M. Zhang, Y. G. Li, Y. Q. Gao and E. B. Wang, *Chem. Commun.*, 2014, **50**, 6017-6019.
12 Nohra, B.; Moll, H. E.; Rodriguez-Albelo, L. M.; Mialane, P.; Marrot, J.; Mellot-Draznieks, C.; O'Keeffe, M.; Biboum, R. N.; Lemaire, J.; Keita, B.; Nadjo, L.; Dolbecq, A. *J. Am. Chem. Soc.*, 2011, **133**, 13363−13374.
13 X. L. Wang, J. J. Sun, H. Y. Lin, Z. H. Chang, A. X. Tian, G. C. Liu and X. Wang, *Dalton Trans.*, 2016, **45**, 2709–2719; X. L. Wang, Z. H. Chang, H. Y. Lin, A. X. Tian, G. C. Liu, J.W. Zhang and D. N. Liu, *CrystEngComm.*, 2015, **17**, 895–903.
14 X. L. Wang, H. L. Hu, G. C. Liu, H. Y. Lin, A. X. Tian, *Chem. Commun*. 2010, **46**, 6485−6487.
15 Y. C. Wang, F. Y. Li, L. Xu, N. Jiang and X. Z. Liu, *Dalton Trans.*, 2013, **42**, 5839–5847.
16 F. Y. Li, F. Z. Meng, L. F. Ma, L. Xu, Z. X. Sun and Q. Gao, *Dalton Trans.*, 2013, **42**, 12079–12082.
17 C. Y. Sun, S. X. Liu, D. D. Liang, K. Z. Shao, Y. H. Ren, Z. M. Su, *J. Am. Chem. Soc.*, 2009, **131**, 1883−1888.
18 S. T. Zheng, J. Zhang, G. Y. Yang, *Angew. Chem., Int. Ed.*, 2008, **47**, 3909−3913.
19 W. Q. Kan, J. F. Ma, Y. Y. Liu, H. Wu, J. Yang, *CrystEngComm.*, 2011, **13**, 7037; G. F. Hou, L. H. Bi, B. Li, L.X. Wu, *Inorg. Chem.*, 2010, **49**, 6474; Y. Q. Lan, S. L. Li,

View Article Online
DOI: 10.1039/C7DT01302G

X. L. Wang, K. Z.Shao, D. Y. Du, H. Y. Zang, Z. M. Su, *Inorg. Chem.*, 2008, **47**, 8187; X. L. Wang, Z. H. Chang, H. Y. Lin, A. X. Tian, G. C. Liu and J. W. Zhang, *Dalton Trans.*, 2014, **43**, 12272–12278; A. X. Tian, Y. Yang, J. Ying, N. Li, X. L. Lin, J. W. Zhang and X. L. Wang, *Dalton Trans.*, 2014, **43**, 8405–8413.

20 H. Y. An, L. Wang, Y. Hu and F. Fei, *CrystEngComm.*, 2015, **7**, 1531; F. Fei, H. Y. An, T. Q. Xu and C. G. Meng, *RSC Adv.*, 2016, **6**, 92092–92103.

21 H. Y. An, Y. Hu, L. Wang, E. L. Zhou, F. Fei and Z. M. Su, *Cryst. Growth. Des.*,2015, **15**, 164−175.

22 B. L. Fei, W. Li, J. H. Wang, Q. B. Liu, J. Y. Long, Y. G. Li, K. Z. Shao, Z. M. Su and W. Y. Sun, *Dalton Trans.*, 2014, **43**, 10005–10012.

23 K. Y. Cui, F. Y. Li, L.Xu, Y. C. Wang, Z. X. Sun and H. G. Fu, *CrystEngComm.*, 2013, **15**, 4721–4729.

24 T. T. Basiev, A. A. Sobol, Y. K. Voronko. *Opt Mater.*, 2000, **15**, 205-216.

25 S. B. Mikhrin, A. N. Mishin, A. S. Potapov. *Nucl Instrum Methods Phys Res, Sect A.*, 2002, **486**, 295-297.

26 E. Guermen, E. Daniels, J. S. King. *J. Chem. Phys.*, 1971, **55**, 1093–1097.

27 R. F. D'Vries, M. Iglesias, N. Snejko, E. Gutiérrez-Puebla and M. A. Monge, *Inorg. Chem.*, 2012, **51**, 11349; R. F. D'Vries, V. A. Peña-O'Shea, N. Snejko, M. Iglesias, E. Gutiérrez-Puebla and M. A. Monge, *Cryst. Growth Des.*, 2012, **12**, 5535.

28 M. North, D. L. Usanov and C. Young, *Chem. Rev.*, 2008, **108,** 5146.

29 B. Y. Park, K. Y. Ryu, J. H. Park, S. Lee, *Green Chem.*, 2009, **11**, 946; N. Kurono, M. Yamaguchi, K. Suzuki, T. Ohkuma, *J. Org. Chem*., 2005, **70**, 6530; S. Matsubara, T. Takai, K. Utimoto, *Chem. Lett.*, 1991, 1447; R. Noyori, S. Murata, M. Suzuki, *Tetrahedron.*, 1981, **37**, 3899.

30 Y. Ogasawara, S. Uchida, K. Yamaguchi, N. Mizuno, *Chem. Eur. J.*, 2009, **15**, 4343; K. Iwanami, J.-C. Choi, B. Lu, T. Sakakura, H. Yasuda, *Chem. Commun.*, 2008, 1002; B. Karimi, L. Ma'Mani, *Org. Lett.*, 2004, **6**, 4813; K. Higuchi, M. Onaka, Y. Izumi, *Bull. Chem. Soc. Jpn*., 1993, **66**, 2016.

31 C. L. Hill, C. M. Prosser-McCartha, *Coord. Chem. Rev.*, 1995,**143**, 407; T. Okuhara, N. Mizuno, M. Misono, *Adv. Catal.*, 1996, **41**, 113; R. Neumann, Prog. *Inorg. Chem.* 1998, **47**, 317;Thematic issue on polyoxometalates: C. L. Hill, *Chem. Rev.*, 1998, **98**, 1–390; I. V. Kozhevnikov, Catalysis by Polyoxometalates,*Wiley, Chicheste.r,* 2002.

32 Y. Ogasawara, S. Itagaki, K. Yamaguchi, N. Mizuno, *ChemSus-Che.*, 2011, **4**, 519.

33 Y. J. Kikukawa, K. Suzuki, M. Sugawa, T. Hirano, K. Kamata, K. Yamaguchi, and N. Mizuno. *Angew. Chem. Int. Ed.*, 2012, **51**, 3686–3690; K. Suzuki, M. Sugawa, Y. Kikukawa, K. Kamata, K. Yamaguchi and N. Mizuno. *Inorg. Chem.*, 2012, **51**, 6953.

34 Q. Y. Liu, Y. L. Wang, Z. M. Shan, R. Cao, Y. L. Jiang, Z. J. Wang, and E. L. Yang. *Inorg. Chem.*, 2010, **49**, 8191–8193; X. Q. Yao, M. D. Zhang, J. S. Hu, Y. Z. Li, Z. J. Guo, and H. -G. Zheng; *Cryst. Growth Des.*, 2011, **11**, 3039–3044; O. Botezat, J. v. Leusen, V. Kravtsov, I. G. Filippova, J. Hauser, M. Speldrich, R. P. Hermann, K. W. Krämer, S. X. Liu, S. Decurtins, P. Kögerler, and S. G. Baca. *Cryst. Growth Des.*, 2014, **14,** 4721−4728.

35 Q. X. Han, X. P. Sun, J. Li, P. T. Ma and J. Y. Niu, *Inorg. Chem.*, 2014, **53**, 6107.

36 T. P. Hu, Y. Q. Zhao, Z. Jagličić, K. Yu, X. P. Wang, and D. Sun. *Inorg. Chem.*, 2015, **54**, 7415−7423.

37 G. M. Sheldrick, SHELXL 97, Program for Crystal Structure Refinement, University of Gőttingen, Germany, 1997; G. M. Sheldrick, SHELXL 97, *Program for Crystal Structure Solution, University of Gőttingen, Germany,* 1997.

38 G. A. Tsigdinos, Ph.D. Thesis, *Boston University,* 1961; A. L. Nolan, R. C. Burns and G. A. Lawrance, *Dalton Trans*., 1996, 2629; U. Lee and H. C. Joo, *Acta Cryst*., 2010, **66**, 10.

39 H. T. Evans and J. S. Showell, *J. Am. Chem. Soc.*, 1969, **91**, 6881.

40 I. Creaser, M. C. Heckel, R. J. Neitz, and M. T. Pope. *Inorg. Chem.*, 1993, **32**, 1573- 1578; Q. H. Luo, R. C. Howell, M. Dankova, J. Bartis,C. W. Williams, W. D. Horrocks, V. G. Young, A. L. Rheingold, L. C. Francesconi, and M. R. Antonio. *Inorg. Chem.*, 2001, **40**, 1894-1901; K. Yu, B. Wan, Y. Yu, L. Wang, Z. H. Su, C. M. Wang, C. X. Wang and B. B. Zhou. *Inorg. Chem.*, 2013, **52**, 485−498.

41 C. I. Cabello, F. M. Cabrerizo, A. Alvarez and H. J. Thomas, *J. Mol. Catal. A: Chem.*, 2002, **186**, 89.

42 I. D. Brown, D. Altermatt, *Acta. Crystallogr., Sect. B* 1985, **41**, 244−247.

43 B. Keita, E. Abdeljalil, F. Girard, S. Gerschwiler, L. Nadjoand R. Contant, *J. Solid State Electrochem.*, 1999, **3**, 446; C. Allain, S. Favette, L. M. Chamoreau, J. Vaissermann, L. Ruhlmann, and B. Hasenknopf. *Eur. J. Inorg. Chem.*, 2008, 3433–3441.

44 A. Nicoara, A. Patrut, D. Margineanu, A. Muller. *Electrochemistry Communications.*, 2003, **5**, 511 – 518.

45 M. Giedyk, H. Shimakoshi, K. Goliszewska, D. Gryko and Y. Hisaeda. *Dalton Trans.*, 2016, **45**, 8340–8346; C. Zúñiga, F. Tasca, S. Calderon, D. Farías, F. J. Recio, J. H. Zagal. Journal of *Electroanalytical Chemistry.*, 2016, **765**, 22–29.

46 M. Ibrahim, A. Haider, Y. H. Lan, B. S. Bassil, A. M. Carey, R. J. Liu, G. J. Zhang, B. Keita, W. H. Li, G. E. Kostakis, A. K. Powell and U. Kortz. *Inorg. Chem.*, 2014, **53**, 5179−5188.

47 *Y. Kim and S. Shanmugam. ACS Appl. Mater. Interfaces.,*2013, **5**, 12197−12204.

48 E. L. Zhou, C. Qin, X. L. Wang, K. Z. Shao and Z. M. Su. *CrystEngComm.*, 2016, **18**, 6370.

49 Y. W. Li, L. Y. Guo, H. F. Su, M. Jagodič, M. Luo, X. Q. Zhou, S. Y. Zeng,C. H. Tung, D.Sun, and L. S. Zheng. *Inorg. Chem.*,2017, **56** pp 2481–2489.

50 T. P. Hu, Y. Q. Zhao, K. Mei, S. J. Lin, X. P. Wang andD. Sun. *CrystEngComm.*, 2015, **17,** 5947 – 5952

View Article Online
DOI: 10.1039/C7DT01302G

Table of Contents

Evans-Showell-type polyoxometalate constructing novel 3D inorganic architectures with alkaline earth metal linkers: syntheses, structures and catalytic properties

Yujiao Hou, Haiyan An*, Baojun Ding, Yanqin Li

College of Chemistry, Dalian University of Technology, Dalian 116023, P. R. China

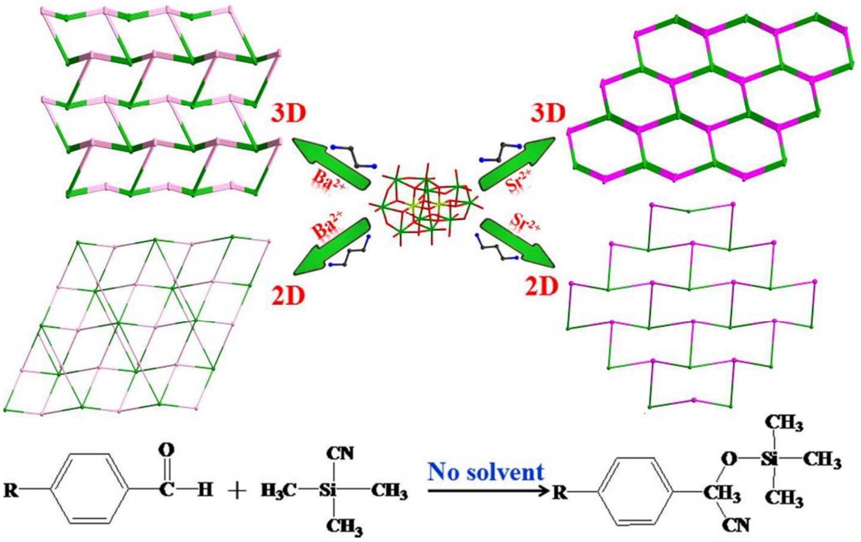

Two 3D frameworks and two 2D networks with excellent catalytic effect of cyanosilylation were successfully obtained, originated from Evans-Showell-type polyoxoanions $[Co_2Mo_{10}H_4O_{38}]^{6-}$ and alkaline earth metal cations (Sr^{2+}, Ba^{2+}).